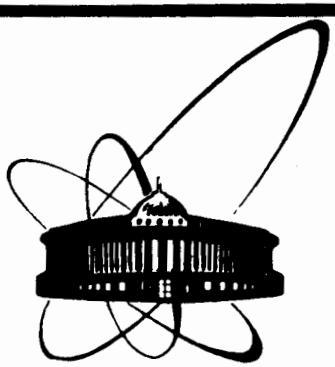

объединенный
институт
ядерных
исследований
дубна

E2-83-464

V.A.Nesterenko, A.V.Radyushkin

QUARK-HADRON DUALITY AND NUCLEON FORM FACTORS IN QCD

Submitted to "Ядерная физика"

1983

1. INTRODUCTION

The quark counting rules (QCD) [1, 2] are now a part of the high energy physics "folk-lore". These rules predict, in particular, that a spin-averaged form factor of a hadron constituted by n quarks should behave asymptotically like t^{1-n} (where $t \equiv Q^2 = -q^2$ and q is the momentum transfer). According to Brodsky and Farrar [2] the specific dynamical mechanism responsible for the QCR is the hard rescattering of quarks that constitute the hadrons participating in the high momentum transfer process. The simple parton-like picture proposed in ref.[2] was justified later within the perturbative QCD framework [3,4]. It was demonstrated, in particular, that in the asymptotic $t \to \infty$ region the QCD-effects produce only a logarithmic violation of the QCR power-law behaviour of the meson and nucleon electromagnetic form factors [3-8].

Experimentally the products $t^2 G^N_{E,M}(t)$ are roughly constant starting with $t \sim 3$ GeV^2. This fact is usually interpreted as an unambiguous indication that for t as low as 3 GeV^2 one observes the asymptotic scaling law corresponding to dominance of the 2-gluon-exchange diagrams like that shown in fig.1c. However, it is not an easy task to justify such an interpretation within the QCD framework. Note, in particular, that the contribution due to diagrams of the type of fig.1c is, in a sense, only the third term of the QCD expansion resulting from applying to $G^N(t)$ the standard procedure of separating long- and short-distance contributions (see Fig.1).

To estimate the relative contributions of figs.1a-c one should take into account, that for $t = 0$ the main contribution to $G^N(t)$ is given by the simplest diagram 1a. Furthermore, according to the usual "loop counting" the higher order diagrams 1b,c are damped by $\left(\frac{a_s(M_N)}{\pi}\right) \lesssim 0.1$ and $\left(\frac{a_s(M_N)}{\pi}\right)^2 \lesssim 0.01$ factors, respectively (M_N is the nucleon mass). This means that there should exist a region $t \lesssim t_{max}$, where the simplest diagram 1a dominates in spite of the fact that in the asymptotic region its contribution vanishes faster than that of fig.1c. According to perturbative estimates (to be justified below) the contribution of fig.1a vanishes only like $1/t^3$, and one should expect that t_{max} is as large as $O((a_s/\pi)^{-2}) \cdot 1$ GeV^2.

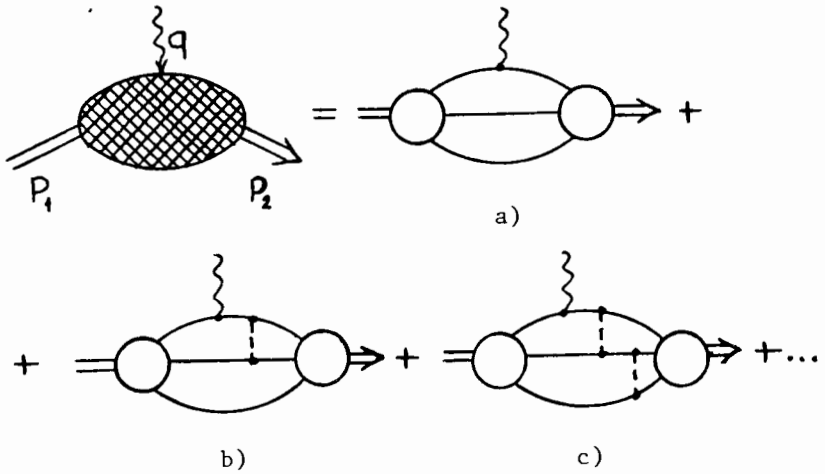

Fig.1. Factorization expansion for the nucleon form factors. Blobs and the quark lines directly attached to them correspond to long distances (small virtualities), whereas the remaining quark and gluon lines to short distances, i.e. to virtualities larger than typical hadronic scale $\mu^2 \sim 1$ GeV^2.

To get a more reliable estimate of the contributions of figs. 1a-c., one should know the soft nucleon wave function. This task cannot of course be solved by using the ordinary perturbation theory, since the very existence of hadrons in QCD is largely due to nonperturbative effects.

In the present paper, to study the behaviour of the nucleon form factors at moderately large momentum transfers, we incorporate the quark-hadron duality concept [9-15] that (in various formulations)has successfully been applied earlier to the computation of such essentially nonperturbative hadron characteristics as masses, leptonic widths, and more recently, electromagnetic form factors of mesons [12-14]. We shall observe below that the contribution of the simplest diagram 1a is in a very good agreement with the existing experimental data. Hence, contrary to the current folk-lore, the experimental verification of the QCR power law does not imply that the main contribution in the relevant t-region is due to diagrams involving a short-distance subprocess.

2. QUARK-HADRON DUALITY

Consider the three-point function

$$T^{\mu}_{\alpha\beta}(p_1, p_2) = i^2 \int d^4x d^4y \exp\{ip_2 x - iqy\} \langle 0| T\{\eta_\alpha(x) J_\mu(y) \bar{\eta}_\beta(0)\}|0\rangle, \quad (1)$$

where $q = p_2 - p_1$, J_μ is the electromagnetic current and η_α is a 3-quark current having a non-zero projection onto the nucleon state $|P\rangle$

$$\langle 0|\eta_\alpha(0)|P\rangle = \lambda_N v_\alpha(P), \quad (2)$$

$v_\alpha(P)$ being the Dirac spinor. A possible choice for the proton is [10]

$$\eta = (u^a C^{-1} \gamma_\lambda u^b)\gamma_5 \gamma^\lambda d^c \epsilon_{abc} \quad (3)$$

with $u \leftrightarrow d$ for the neutron; C being the charge conjugation matrix.

The amplitude $T^{\mu}_{\alpha\beta}$ is the sum of various structures: $P^\mu(\hat{P})_{\alpha\beta} \equiv V^{\mu}_{\alpha\beta}(P)$; $q^\mu(\hat{P})_{\alpha\beta}$; $Q^2(\gamma^\mu)_{\alpha\beta}$; $i\epsilon^{\mu\lambda\rho\sigma} P_\lambda q_\rho(\gamma_5\gamma_\sigma) \equiv A^{\mu}_{\alpha\beta}(P,q)$,etc., where $P = p_1 + p_2$.To compare the contributions of different structures, one should specify the reference frame. In our case very convenient is the infinite momentum frame (IMF), where $P^\mu \equiv p^\mu_\parallel \to \infty$ while $q^\mu \equiv q^\mu_\perp$ is fixed. The leading IMF structure is clearly $V^{\mu}_{\alpha\beta}(P)$: it does not contain the "small" parameter q. Note that for $p_1^2 = p_2^2$ the $V^{\mu}_{\alpha\beta}$-structure satisfies the transversality condition $q_\mu V^{\mu}_{\alpha\beta}(P) = 0$. Another structure possessing this property is $A^{\mu}_{\alpha\beta}(P, q)$. These two structures have a most direct connection with the $(\hat{P})_{\alpha\beta}$ -component of the two-point function $\Pi_{\alpha\beta}(P)$

$$\Pi_{\alpha\beta}(P) = i \int d^4x \exp(iPx) \langle 0| T\{\eta_\alpha(x) \bar{\eta}_\beta(0)\}|0\rangle \quad (4)$$

analysed in refs. [10,15].

The invariant amplitudes related to the $V^{\mu}_{\alpha\beta}$- and $A^{\mu}_{\alpha\beta}$ -structures will be denoted as T_V and T_A, respectively. To incorporate the quark-hadron duality, we write the double dispersion relation for $T_{V,A}(p_1^2, p_2^2, t)$

$$T_i(p_1^2, p_2^2, t) = \frac{1}{\pi^2} \int_0^\infty ds_1 \int_0^\infty ds_2 \frac{\rho_i(s_1, s_2, t)}{(s_1 - p_1^2)(s_2 - p_2^2)} + \dots, \quad (5)$$

where the terms not written explicitly are polynomials in p_1^2 and/or p_2^2.

The perturbative contribution to $T_i(p_1^2, p_2^2, t)$ (corresponding, e.g., to figs. 1a-c with the blobs substituted by local vertices dictated by the $\eta, \bar{\eta}$ -currents) can also be written in the form of eq. (5). Of course, the perturbative spectral density $\rho^{pert}(s_1, s_2, t)$ differs from the physical density $\rho(s_1, s_2, t)$ especially for small s_1, s_2 values. In particular, $\rho(s_1, s_2, t)$ contains the nucleon $\delta\delta$ -term

$$\rho_i^N(s_1, s_2, t) = \pi^2 \lambda_N^2 \mathcal{F}_i^N(t) \delta(s_1 - M_N^2) \delta(s_2 - M_N^2) \qquad (6)$$

while the finite-order contributions to $\rho^{pert}(s_1, s_2, t)_N$ are smooth functions of s_1, s_2. We shall assume, however, that $\rho_i^N(s_1, s_2, t)$ is dual to $\rho_i^{pert}(s_1, s_2, t)$

$$\int_0^{s_0} ds_1 \int_0^{s_0} ds_2 \rho_i^{pert}(s_1, s_2, t) = \int_0^{s_0} ds_1 \int_0^{s_0} ds_2 \rho_i^N(s_1, s_2, t) = \lambda_N^2 \mathcal{F}_i^N(t), \qquad (7)$$

where the duality interval s_0 characterizes the onset of the "continuum" in the η-channel, i.e., the effective threshold for higher states with the quantum numbers of η. The specific value $s_0 = 2.3$ GeV^2 that will be used in what follows has been extracted in ref. [15] from a detailed analysis of the power corrections in the exponential-weighted ("borelized") QCD sum rules for the $(P)_{\alpha\beta}$ -component of the correlator $\Pi_{\alpha\beta}(P)$.

It is worth emphasizing that in the local duality approximation there exists a simple relation between s_0 and the proton decay constant λ_N, e.g., in the lowest order

$$(2\pi)^4 \lambda_N^2 = \frac{s_0^3}{12}. \qquad (8)$$

As a result, the predictions based on eq. (7) do not contain free parameters.

3. LOCAL DUALITY AND THE SOFT NUCLEON WAVE FUNCTION

Incorporating the local duality ansatz (7) is equivalent to fixing the soft nucleon wave function (s.w.f.). Indeed, taking into account that $\rho_i^{pert}(s_1, s_2, t)$ is the double discontinuity (in p_1^2 and p_2^2) of the relevant amplitude $T_i(p_1^2, p_2^2, t)$, it is easy to realize that for fig.1a the use of the eq. (7) prescription reduces to replacing the s.w.f. by a local vertex corresponding to transition of the η-current into free, almost massless*

* Calculating $\rho^{pert}(s_1, s_2, t)$ one should use, of course, the current quark masses, $m_u, m_d \lesssim 10$ MeV $\ll M_N, \sqrt{s_0}$.

quarks with a subsequent averaging of the invariant mass s of the 3-quark system over the region $0 \le s \le s_0$. In other words, the nucleon is treated as a system composed of 3 on-shell $(k_i^2 = m_q^2)$ quarks localized inside a sphere $(k_1 + k_2 + k_3)^2 \le s_0$ in the momentum space. This picture, in particular, has a merit of being both relativistically and gauge invariant.

It is instructive to observe that in the infinite momentum frame (IMF) such a wave function is proportional to $\theta(\kappa^2 < s_0)$, κ^2 being the usual IMF combination (cf. ref. [6])

$$\kappa^2 = \sum_{i=1}^{3} \frac{k_{i\perp}^2}{x_i}, \qquad (9)$$

where x_i is the IMF fraction of the nucleon longitudinal momentum carried by the i-th quark, and $k_{i\perp}$ is its transverse momentum. It is worth comparing now the wave function $\Psi^{(LD)}(k_{\perp i}, x_i) \sim \theta(\kappa^2 < s_0)$, suggested by the local quark-hadron duality, with the Gaussian $\Psi^{(G)}(k_{\perp i}, x_i) \sim \exp(-R^2 \kappa^2)$ and power-law $\Psi^{(PL)}(k_{\perp i}, x_i) \sim (\kappa^2 + \mu^2)^{-\alpha}$ model wave functions considered by Brodsky and Lepage [16]. All the wave functions have a common property: the cut-off for large κ^2 values. Of course, the sharp cut-off $\kappa^2 \le s_0$ dictated by $\Psi^{(LD)}(k_{\perp i}, x_i)$ is unrealistic: the exact nucleon s.w.f. should be a smooth function of κ^2, like $\Psi^{(G)}(k_{\perp i}, x_i)$ or $\Psi^{(PL)}(k_{\perp i}, x_i)$.

Thus, $\Psi^{(LD)}(k_{\perp i}, x_i)$ can reproduce only the most general (i.e., integral) properties of the exact nucleon soft wave function. Correspondingly, one should not expect that $G_i^{(N)}(t)$ calculated according to eq. (7) must coincide with the exact contribution of fig. 1a in the whole region $0 < t < \infty$. In particular, one should not trust eq. (7) predictions in the t -regions where its contribution has an essential dependence on the specific behaviour of the s.w.f. on the edges of the kinematically allowed region, when $x_i \sim 0$ or 1 for some i.

As we will see later, (eqs. (11), (12)) the behaviour of $\rho^{pert}(s_1, s_2, t)$ for small t is rather sensitive to the region $x^{(A)} \sim 0$, where a bulk part of the longitudinal IMF momentum of the nucleon is carried by the passive quarks, while for large t values the dominant contribution to $\rho^{pert}(s_1, s_2, t)$ is due to integration over the region $x^{(A)} \sim 1$ where the nucleon momentum is carried mainly by the active quark. Thus, one should rely on eq. (7) predictions neither for very small nor for asymptotically large t values.

A more quantitative estimate of the applicability region of eq. (7) may be obtained in the following way. Note, firstly, that the perturbative calculations for the original amplitude $T_i(p_1^2, p_2^2, t)$ are reliable only within the asymptotic freedom region $t \gtrsim m_\rho^2 \sim 0.6$ GeV^2. A next observation is that the asymp-

totic $t \to \infty$ behaviour of $T_i(p_1^2, p_2^2, t)$ is dominated by the region where the off-shellnesses of the spectator quarks are of order $(p^2)^2/t$. Hence, for $t \to \infty$ we leave the asymptotic freedom region again. Noting that in eq. (7) the p^2-parameter is substituted effectively by s_0 we deduce that the upper bound on the applicability region of eq. (7) is dictated by the constraint $s_0^2/t \gtrsim m_\rho^2$. In our case $s_0 = 2.3$ GeV^2, $m_\rho^2 = 0.6$ GeV^2 and the upper bound is $t \lesssim 10$ GeV^2.

This means that there should exist the intermediate region $0.5\text{-}1 \lesssim t \lesssim 10\text{-}20$ GeV^2 where the contribution of fig.1a is determined just by the integral properties of the s.w.f., mainly by the width of the quark distribution in transverse momentum (i.e., eventually by the nucleon size). The dependence on the specific form of such a distribution in this region is rather weak.

The dimensional parameter that characterizes the width of the $k_\perp$-distribution for $\Psi^{(LD)}(k_{\perp i}, x_i)$ is clearly s_0 (in fact $\langle k_\perp^2 \rangle \sim s_0/10 \sim (500\ \text{MeV})^2$), i.e., the same parameter that sets the scale of the baryon mass spectrum in the η-channel. Such a connection seems to be quite reasonable from a physical standpoint.

4. QUARK-HADRON DUALITY PREDICTIONS FOR THE NUCLEON FORM FACTORS

4.1. General Analysis

The trickiest technical problem in our approach is the calculation of the perturbative spectral density $\rho^{pert}(s_1, s_2, t)$. However, for fig.1a the problem is considerably simplified if one notices that in the configuration space one can treat this diagram as a one-loop graph. Incorporating this observation it is straight-forward to obtain a rather simple integral representation for the Borel transform Φ_i

$$\Phi_i(M_1^2, M_2^2, t) = \frac{1}{\pi^2} \int_0^\infty \frac{ds_1}{M_1^2} \int_0^\infty \frac{ds_2}{M_2^2} \rho_i^{pert}(s_1, s_2, t) \exp\left(-\frac{s_1}{M_1^2} - \frac{s_2}{M_2^2}\right) \quad (10)$$

of the invariant amplitude $T_i(p_1^2, p_2^2, t)$ (details are presented in the Appendix). In particular, for the proton functions $\Phi_V^{(p)}$ and $\Phi_A^{(p)}$ related to V- and A-structures, we obtain for massless quarks

$$\Phi_V^{(p)}(M_1^2, M_2^2, t) = \frac{1}{(2\pi)^4} \frac{(M_1^2 M_2^2)^2}{(M_1^2 + M_2^2)^3} \int_0^1 dx (1-x)^2 \left[2x + \frac{1}{3}(1-x)\right] \exp\left\{-\frac{(1-x)t}{x(M_1^2+M_2^2)}\right\}, \quad (11)$$

$$\Phi_A^{(p)}(M_1^2, M_2^2, t) = \frac{1}{(2\pi)^4} \frac{(M_1^2 M_2^2)^2}{(M_1^2 + M_2^2)^3} \int_0^1 dx 2(1-x)^2 \exp\left\{-\frac{(1-x)t}{x(M_1^2+M_2^2)}\right\}. \quad (12)$$

Note that the x-variable in eqs. (11), (12) is just the IMF fraction of the nucleon momentum carried by the active quark.

Inverting eq. (10) (which is the double Laplace transformation in $1/M^2$) one can get from eqs. (11), (12) explicit expressions for $\rho_{V,A}^{pert}(s_1, s_2, t)$. Substituting the latter into eq. (7) gives for the proton form factors

$$F_V^p(t) = \frac{1}{(2\pi)^4 \lambda_N^2} \int_0^{s_0} ds_1 \int_0^{s_0} ds_2 t\left(1 - \frac{\sigma}{z}\right)^2 \left\{\frac{2e_u - e_d}{16} \frac{t}{z}\left(1 + \frac{\sigma}{z}\right)^2 + \right. \quad (13)$$

$$\left. + \frac{e_u + e_d}{12}\left(2 + \frac{\sigma}{z}\right)\right\},$$

$$F_A^p(t) = \frac{e_u}{(2\pi)^4 \lambda_N^2} \int_0^{s_0} ds_1 \int_0^{s_0} ds_2 \frac{t}{4}\left(1 - \frac{\sigma}{z}\right)^2 \left(2 + \frac{\sigma}{z}\right), \quad (14)$$

where $\sigma = s_1 + s_2 + t$, $z = \sqrt{\sigma^2 - 4s_1 s_2}$, $e_u = 2/3$, $e_d = -1/3$.

To get the neutron form factors one should interchange $e_u \leftrightarrow e_d$ in eqs. (13), (14). To compare eqs. (13), (14) with experimental data one should substitute λ_N^2 by its value given by eq. (8) and take $s_0 = 2.3$ GeV^2. One should also take into account that $F_V(t)$ is a combination of the electric (G_E) and magnetic (G_M) Sachs form factors

$$F_V(t) = \frac{4M_N^2 G_E(t) + t G_M(t)}{t + 4M_N^2}. \quad (15)$$

For small t the r.h.s. of eq. (15) reduces to $G_E(t)$ while for large t (in fact, for $t \gtrsim 10$ GeV^2) it may be treated as $G_M(t)$. The second form factor $F_A(t)$ coincides with $G_M(t)$.

It is easy to derive that as $t \to \infty$ the r.h.s. of eq. (13) tends to that of eq. (14), and the two expressions give the same result $G_M^{p(n)}(t) \sim 4 \cdot e_{u(d)}\, s_0^3/t^3$ for the asymptotic behaviour of the magnetic form factors. It should be emphasized, however, that the asymptotic $O(t^{-3})$ regime for eqs. (13) and (14) sets in only for $t \gtrsim 20\text{-}30$ GeV^2. In fact, the products $t^2 F_V(t)$ and $t^2 G_M(t)$ as predicted by eqs. (13) and (14) are

constant within 10% for t varying from 5 to 15 GeV^2. In other words, eqs. (13) and (14) imitate the power-law behaviour $G_M \sim 1/t^2$ dictated by the QCR [1,2] up to the t-values as large as 20 GeV^2. In higher orders, however, one should take into account also a possible modification of eqs. (13) and (14) for large t by the Sudakov form factor of the struck quarks:

$$S(t, M^2) = \exp\{-\frac{8}{27}[(\ln\frac{t}{\Lambda^2} - \frac{3}{2})\ln(\frac{\ln t/\Lambda^2}{\ln M^2/\Lambda^2}) - \ln\frac{t}{M^2}]\}, \qquad (16)$$

where the scale M^2 is proportional to s_0, the only dimensionful parameter in eqs. (13) and (14). Note, that the value of s_0 is rather large whereas the QCD Λ-parameter is presumably small ($\Lambda \sim 100$ MeV), and as a result, in the accessible region $t \lesssim 20$–30 GeV^2 the Sudakov suppression of eqs. (13) and (14) is not very strong. Furthermore, such a suppression may be partly compensated by contributions of the diagrams 1b,c. Thus, it seems quite reasonable to neglect the higher order corrections for $t \lesssim 20$ GeV^2, and expect in this region a good agreement between the local quark-hadron duality predictions and experimental data.

As for the low t region, an important observation here is that owing to the current conservation the electric form factor $G_E(t)$ calculated from eqs. (13) and (14) takes for $t = 0$ its experimental value (1 for the proton and 0 for the neutron). Furthermore, according to eqs. (11) and (12), both Φ_V and Φ_A are finite for $t = 0$, but $d\Phi_{A,V}/dt|_{t=0}$ (and, as a result $(dF_{A,V}(t)/dt)|_{t=0}$) is infinite for massless quarks. A non-zero quark mass m_q provides the necessary IR cutt-off, and $dF_{A,V}/dt$ is finite for $t = 0$, although very large ($\sim \ln M^2/m_q^2$). Of course, the sensitivity of the prediction to the specific value of the (current) quark mass means that the quantity analyzed is not infrared stable, and one should not rely on perturbation theory to estimate its magnitude. On the phenomenological level the account of the relevant nonperturbative effects reduces to the substitution of m_q by a more realistic IR cut-off like $\mu \sim 1/R_N$, where R_N is the nucleon radius. However, for $t \gtrsim 1$ GeV^2 the IR cut-off is provided by t itself and, as a result, all the derivatives of $F_{A,V}(t)$ are finite and, what is even more important, sufficiently stable with respect to possible variations of m_q.

4.2. Numerical Results

Now we turn to the comparison of the predictions of eqs. (13) and (14) with existing experimental data.

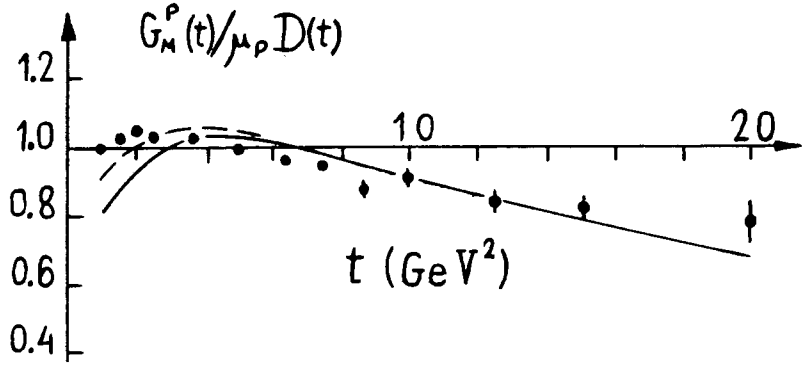

Fig.2. Form factor $G_M^p(t)/\mu_p D(t)$. Solid line corresponds to eq. (14); dashed line – to eq. (13) combined with the assumption that $G_M^p(t)/G_E^p(t) = \mu_p = 2{,}79$.

a). Proton form factors. Note first that $G_M^p(t)$ obtained from eq. (14) in the region $t = 2$–10 GeV^2 is in 10% agreement with the empirical dipole fit $G_M^p(t) = \mu_p D(t)$ (where $\mu_p = 2.79$ and $D(t) = (1 + t/0.71)^{-2}$) (fig.2). Furthermore, using eqs. (13)-(15) one can obtain an explicit expression for $G_E(t)$ and observe that $G_E^p(t) \simeq D(t)$ within 10% for $t \lesssim 12$ GeV^2 (fig.3). As a result, the scaling relation $G_M^p(t)/G_E^p(t) \simeq \mu_p$ holds within 15% for t ranging from 3 to 15 GeV^2. On the other hand, assuming that $G_M^p(t)/G_E^p(t) = \mu_p$ for all t one can extract $G_M^p(t)$ from eq. (13) which is presumably more precise for small t-values than eq. (14)* Indeed, the results for $G_M^p(t)$ obtained in this way are in better agreement with the dipole fit for $t = 1$–2 GeV^2 than those extracted from eq. (14) (fig.2).

b) Neutron magnetic form factor. The predictions of eqs. (13) and (14) for $G_M^n(t)$ agree with the data within the experimental uncertainties only for $t \gtrsim 6$ GeV^2 (fig.4). In the region $t \lesssim 6$ GeV^2 the agreement between the neutron version of eq. (14) and experiment is not so impressive as that for $G_M^p(t)$. In particular the prediction of eq. (14) for the ratio $|G_M^n(t)|/D(t)$ in the $t = 3$–6 GeV^2 region is by 30% lower than that observed experimentally. The disagreement is even more drastic for $t = 1$–2 GeV^2. If one calculates $G_M^n(t)$ from eq. (13) assuming

* Note that the structure $V^{\mu}_{\alpha\beta}$ relevant to eq. (13) has no damping for small q; hence, for small t the original amplitude $T^{\mu}_{\alpha\beta}(p_1, p_2)$ is more sensitive to the contribution of $F_V(t)$ than to that of $F_A(t)$.

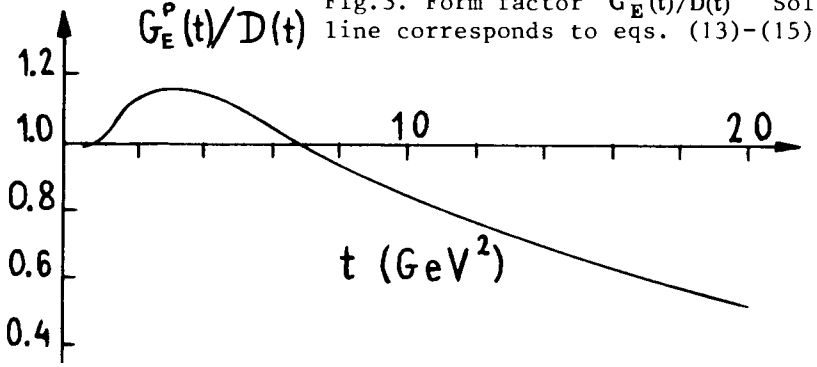

Fig.3. Form factor $G_E^p(t)/D(t)$ Solid line corresponds to eqs. (13)-(15).

that $G_E^n(t) = 0$, then the disagreement between theory and experiment for $t = 1$-4 GeV^2 is reduced, but only to 20%. The situation may be interpreted so that the difference between the exact nucleon w.f. and that suggested by the quark-hadron duality is more essential for $G_M^n(t)$ than for $G_M^p(t)$. It is worth emphasizing here that such a proton-neutron asymmetry does not contradict the isotopic invariance. In particular, studying the power corrections in the (exponential-weighted) QCD sum rules for $G_M(t)$, we have observed that for the proton the most essential $\langle\bar{\psi}\psi\rangle^2$ -corrections are proportional to e_d, while the ground term according to eq. (14) is proportional to e_u. As a result, the ratio of the $\langle\bar{\psi}\psi\rangle^2$-correction to the ground term for the neutron is 4 times as large as that for the proton.

c) Neutron electric form factor and the nucleon mass estimate.

Using eqs. (13)-(15) one can calculate $G_E^n(t)$ and observe that the predicted $G_E^n(t)$-values are very close to zero for $t = 2$-20 GeV^2 (fig.5). It should be stressed here that the smallness of $G_E^n(t)$ reflects a nontrivial correlation between the values of $F_V^n(t), G_M^n(t)$ predicted by eqs. (13) and (14) and the magnitude of the nucleon mass parameter M_N entering into eq. (15). For instance, requiring $G_E^n(t)$ to be exactly zero, one can extract the nucleon mass from eqs. (13)-(15). In the region $t = 2$-30 GeV^2 such a procedure gives for M_N the values very close to the experimental one (see Fig.5).

d) Ratio $G_M^p(t)/G_M^n(t)$

According to eq. (14), the ratio $G_M^p(t)/G_M^n(t)$ equals (-2) for all t. In its turn, eq. (13) (combined with the assumption that $G_E(t)/G_M(t) = G_E(0)/G_M(0)$) predicts that $|G_M^p(t)/G_M^n(t)|$ is smaller than 2 for $t \lesssim 4$ GeV^2 (e.g., 1.6 for $t = 1$ GeV^2), but in the region $t \gtrsim 4$ GeV^2 eq. (13) also gives $G_M^p(t)/G_M^n(t) = -2$.

This prediction agrees well with the recent data [17] in the $t \gtrsim 6$ GeV^2 region.

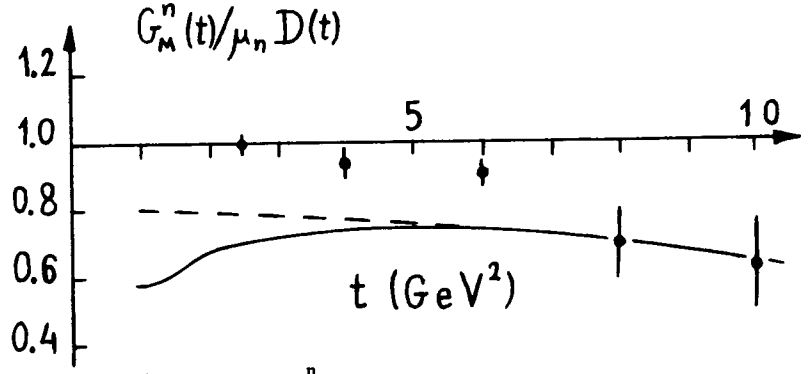

Fig.4. Form factor $G_M^n(t)/\mu_n D(t)$. Solid line corresponds to eq. (14); dashed line - to eq. (13) combined with the assumption that $G_E^n(t) = 0$.

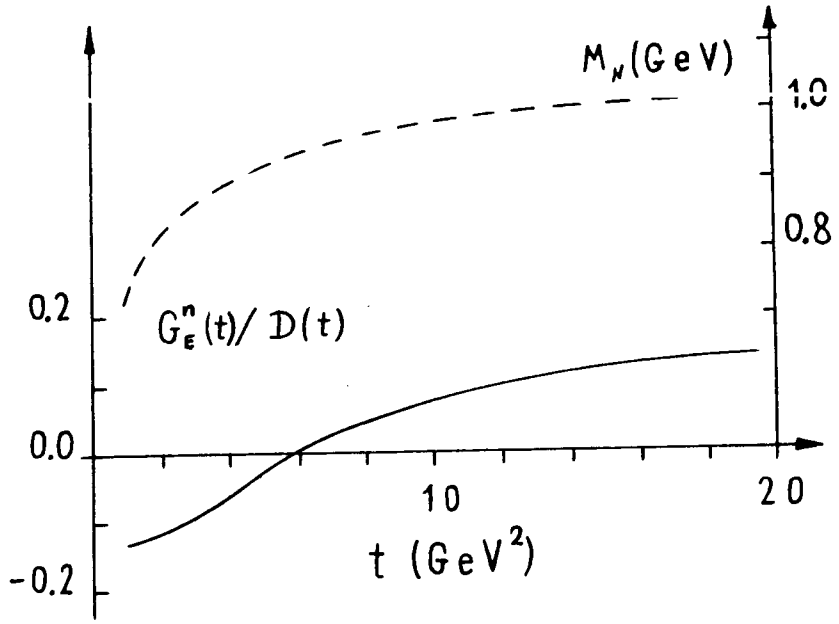

Fig.5. Left scale: form factor $G_E^n(t)/D(t)$. Right scale: nucleon mass extracted from eqs. (13)-(15) assuming that $G_E^n(t) = 0$.

e) Magnetic Moments

As emphasized earlier, there are no grounds to expect eq. (14) to agree with the experimental data in the region $t \lesssim 1\ \mathrm{GeV}^2$. However, the values of magnetic moments $\mu_p = G_M^p(0) = 4e_u = 8/3$ and $\mu_n = G_M^n(0) = 4e_d = -4/3$ predicted by eq. (14) are in satisfactory agreement with the experimental ones. Note, that just like it was for $t \gtrsim 1\ \mathrm{GeV}^2$, the model is more successful for the proton than for the neutron. It is intriguing to observe also that the ratio $(|\mu_n| - 4/3)/(\mu_p - 8/3)$ is indeed close to 4.

5. CONCLUSIONS

Thus, in a rather wide region of $t = 2\text{-}15\ \mathrm{GeV}^2$ the nucleon form factors calculated according to the local quark-hadron duality prescription are in satisfactory (or even good) agreement with the experimental data. One of the most nontrivial results here is that the ratio $G_M^p(t)/G_M^n(t)$ for sufficiently large t is predicted by eqs. (13) and (14) to take just the value (-2) suggested by the recent experimental data [17].

Modifying the s.w.f. in an appropriate way (this is achieved by adding to the η-current (eq. (1)) the terms containing covariant derivatives), it is possible to extend the agreement between the fig. 1a contribution and the experimental data to higher t values. However, in the present paper such a modification was not attempted. We concentrated rather on the preasymptotic region $t \lesssim 20\ \mathrm{GeV}^2$ where the local duality predictions are less sensitive to a particular choice of the η-current. As we have observed, just in this region eqs. (13) and (14) do successfully describe the data. This observation forces us to conclude: the experimentally observed power-law fall-off of the nucleon form factors reflects only the finite size of the nucleons rather than the approximate short-distance scale invariance of the underlying field theory.

6. ACKNOWLEDGEMENT

We are grateful to A.V.Efremov, V.A.Meshcheryakov, and D.V.Shirkov for interest in this work and support.

APPENDIX. Calculation of $\Phi^p(M_1^2, M_2^2, t)$

The first step is to write the contribution of the fig. 1a diagram in the configuration representation and then to calculate the trace. This gives

$$T^{\mu}_{\alpha\beta}(p_1, p_2) = \frac{64}{(2\pi)^4} \int d^4x\, d^4y \exp\{ip_1 x - iqy\} \times$$

$$\times \{\gamma^{\mu}\left[\frac{1}{x^6 y^4 (x-y)^2} + \frac{1}{x^6 y^2 (x-y)^4} - \frac{1}{x^4 y^4 (x-y)^4}\right] +$$

$$+ \frac{\hat{x}\, x^{\mu}}{x^8 y^2 (x-y)^4} + 2\frac{\hat{y}\, x^{\mu}}{x^6 y^4 (x-y)^4} - 4\frac{\hat{y}\, y^{\mu}}{x^6 y^4 (x-y)^4} + \qquad (A.1)$$

$$+ \hat{x}\, y^{\mu}\left[\frac{1}{x^8 y^4 (x-y)^2} - \frac{1}{x^8 y^2 (x-y)^4} + \frac{2}{x^6 y^4 (x-y)^4}\right] -$$

$$- 2i\gamma^5 \gamma_{\delta}\, \epsilon^{\mu\kappa\sigma\delta}\, \frac{x^{\kappa} y^{\sigma}}{x^6 y^4 (x-y)^4}\}.$$

The next step is to introduce the α-representation for the denominator factors $x^2, y^2, (x-y)^2$:

$$\frac{1}{(z^2)^N} = \frac{i^N}{(N-1)!} \int_0^{\infty} \frac{d\alpha}{\alpha^{N+1}} \exp\{-i\frac{z^2}{\alpha}\} \qquad (A.2)$$

and then to perform integration over x and y. After this has been done, the tensor structure of $T^{\mu}_{\alpha\beta}$ is explicit, and each invariant amplitude $T_i(p_1^2, p_2^2, t)$ has the α-representation of the form

$$T_i^p(p_1^2, p_2^2, t) = \int_0^{\infty} d\alpha d\beta d\gamma\, f_i(\alpha, \beta, \gamma) \times \qquad (A.3)$$

$$\times \exp\{p_1^2 \frac{\alpha\gamma}{\alpha+\beta+\gamma} + p_2^2 \frac{\beta\gamma}{\alpha+\beta+\gamma} - t\frac{\alpha\beta}{\alpha+\beta+\gamma}\}.$$

To get the double Borel transform $\Phi_i^p(M_1^2, M_2^2, t)$ (see eq. (10)) we must apply to $T_i^p(p_1^2, p_2^2, t)$ the SVZ operator [9]

$$\hat{B}(p^2, M^2) = \lim_{n\to\infty} \frac{(-p^2)^n}{(n-1)!} \left(\frac{d}{dp^2}\right)^n \Big|_{p^2 = -nM^2} \qquad (A.4)$$

in p_1^2 and p_2^2. This can be easily done using the formula

$$\hat{B}(p^2, M^2)\,[\exp(Ap^2)] = \delta(1 - AM^2)\,. \qquad (A.5)$$

Finally, denoting $x = (\alpha + \beta)/(\alpha + \beta + \gamma)$ we obtain

$$\{\hat{B}(p_1^2, M_1^2)\,\hat{B}(p_2^2, M_2^2)\}\,T^{\mu}_{\alpha\beta}(p_1, p_2) =$$

$$= \frac{1}{(2\pi)^4}\,\frac{(M_1^2 M_2^2)^2}{(M_1^2 + M_2^2)^3}\int_0^1 dx\,(1-x)^2 \exp\{-\frac{(1-x)\,t}{x(M_1^2 + M_2^2)}\}\,. \times$$

$$\times \{\gamma_\mu [-\frac{10}{3}(1-x)\frac{M_1^2 M_2^2}{M_1^2 + M_2^2} - 2t\,\frac{1}{x}] +$$

$$+ \hat{q} P^\mu \frac{5}{3}(1-x)\frac{M_2^2 - M_1^2}{M_1^2 + M_2^2} + \qquad (A.6)$$

$$+ \hat{q}\, q^\mu [-2\frac{1}{x} + \frac{5}{3}\frac{(1-x)^2}{x} - \frac{20}{3}(1-x)(5x-1)\frac{M_1^2 M_2^2}{t(M_1^2 + M_2^2)}] +$$

$$+ \hat{P} P^\mu [2x + \frac{1}{3}(1-x)] +$$

$$+ \hat{P} q^\mu (1-x)(2 + \frac{1}{3}\frac{(1-x)}{x})\frac{M_2^2 - M_1^2}{M_2^2 + M_1^2} +$$

$$+ 2i\gamma_5 \gamma^\delta P_\sigma q_\rho \epsilon^{\mu\sigma\rho\delta}\}\,.$$

REFERENCES

1. Matveev V.A., Muradyan R.M., Tavkhelidze A.N. Lett.Nuovo Cim., 1973, 7, p. 719.
2. Brodsky S.J., Farrar G.R. Phys.Rev.Lett., 1973, 31, p. 1153.
3. Radyushkin A.V. JINR, P2-10717, Dubna, 1977.
4. Brodsky S.J., Lepage G.P. SLAC-Pub-2294, Stanford, 1979.
5. Efremov A.V., Radyushkin A.V. Phys.Lett. B, 1980, 94, p. 245.
6. Brodsky S.J., Lepage G.P. Phys.Rev.D, 1980, 22, p. 2157.

7. Chernyak V.L. Proc. of XV LINP Winter School, Leningrad, 1980, vol. 1, p. 65.
8. Mueller A.H. Phys.Reports, 1981, 73, p. 237.
9. Shifman M.A., Vainshtein A.I., Zakharov V.I. Nucl.Phys.B, 1979, 147, p. 385, 447.
10. Ioffe B.L. Nucl.Phys. B, 1981, 188, p. 317.
11. Krasnikov N.V., Pivovarov A.A. Phys.Lett. B, 1982, 112, p. 397.
12. Nesterenko V.A., Radyushkin A.V. JETP Lett., 1982, 35, p. 486; Phys.Lett. B, 1982, 115, p. 410.
13. Ioffe B.L., Smilga A.V. Phys.Lett. B, 1982, 114, p. 353; Nucl.Phys. B, 1983, 216, p. 373.
14. Nesterenko V.A., Radyushkin A.V. JINR, P2-82-691, Dubna, 1982.
15. Belyaev V.M., Ioffe B.L. JETF, 1982, 83, p. 876.
16. Brodsky S.J., Lepage G.P. SLAC-Pub-2605, Stanford, 1980.
17. Rock S. et al. SLAC-Pub-2949, Stanford, 1982.

Received by Publishing Department
on July 1,1983.

Нестеренко В.А., Радюшкин А.В. E2-83-464

Кварк-адронная дуальность и формфакторы нуклонов в КХД

Кварк-адронная дуальность используется для оценки непертурбативного $O(a_s^0)$-вклада в нуклонные формфакторы $G^N(t)$. Полученные результаты удовлетворительно согласуются с экспериментальными данными в области $1 < t < 20$ ГэВ^2. Это означает, что наблюдаемое дипольное поведение нуклонных формфакторов вовсе не связано с характером динамики на малых расстояниях.

Работа выполнена в Лаборатории теоретической физики ОИЯИ.

Препринт Объединенного института ядерных исследований. Дубна 1983

Nesterenko V.A., Radyushkin A.V. E2-83-464

Quark-Hadron Duality and Nucleon Form Factors in QCD

Quark-hadron duality is incorporated to estimate the non-perturbative $O(a_s^0)$ -contribution to the nucleon form factors $G^N(t)$. For $1 < t < 20$ GeV^2 the results are in satisfactory agreement with the existing data. This means that the observed dipole behaviour of $G^N(t)$ has nothing to do with the short-distance dynamics.

The investigation has been performed at the Laboratory of Theoretical Physics, JINR.

Preprint of the Joint Institute for Nuclear Research. Dubna 1983